The Astrophysical Journal, 677:1–11, 2008 April 10

IMPROVED CONSTRAINTS ON THE ACCELERATION HISTORY OF THE UNIVERSE AND THE PROPERTIES OF THE DARK ENERGY

Ruth A. Daly
Department of Physics, Penn State University, Berks Campus, P. O. Box 7009, Reading, PA 19610; rdaly@psu.edu

S. G. Djorgovski
Division of Physics, Mathematics, and Astronomy, California Institute of Technology, MS 105-24, Pasadena, CA 91125

Kenneth A. Freeman and Matthew P. Mory
Department of Physics, Penn State University, Berks Campus, P. O. Box 7009, Reading, PA 19610

and

C. P. O'Dea, P. Kharb, and S. Baum
Rochester Institute of Technology, 54 Lomb Memorial Drive, Rochester, NY 14623
Received 2007 June 19; accepted 2007 December 17

ABSTRACT

We extend and apply a model-independent analysis method developed earlier by Daly & Djorgovski to new supernova, radio galaxy, and galaxy cluster samples to study the acceleration history of the universe and the properties of the dark energy. There is good agreement between results obtained with radio galaxies and supernovae, suggesting that both distance indicators are reliable. The deceleration parameter $q(z)$ is obtained assuming only the validity of the FRW metric, allowing for a range of values of space curvature, and independent of a gravity theory and the physical nature of the contents of the universe. We show that q_0 is independent of space curvature, and obtain $q_0 = -0.48 \pm 0.11$. The transition redshift when $q_0 = 0$ is $z_T = 0.78^{+0.08}_{-0.27}$ for zero space curvature, and has a weak dependence on space curvature. We find good agreement between model-independent quantities and those predicted by general relativity, indicating that GR provides a good description of the data over look-back times of ten billion years.

Subject headings: cosmological parameters — cosmology: observations — cosmology: theory — dark matter — equation of state

Online material: machine-readable table

1. INTRODUCTION

Understanding the physical nature of the dark energy which appears to be driving the accelerated expansion of the universe is among the most pressing and important topics in cosmology today. Studies of the expansion history of the universe allow us to constrain the physical nature of its matter and energy constituents. One way that the expansion and acceleration history of the universe can be studied is through the use of a set of coordinate distances and redshifts for some standard set of objects. Type Ia supernovae provide a modified standard candle (e.g., Phillips 1993; Hamuy et al. 1995) and powerful radio galaxies provide a modified standard yardstick (Daly 1994; Daly et al. 2008) that allow the distance modulus, luminosity distance, and coordinate distance to each source to be determined. The recent data sets presented by Astier et al. (2006), Riess et al. (2007), Wood-Vasey et al. (2007), Davis et al. (2007), and Daly et al. (2008) have been analyzed by these groups and compared with models by other researchers.

In a novel, largely model-independent approach to this problem, it was shown by Daly & Djorgovski (2003) that the first and second derivatives of the coordinate distance with respect to redshift could be obtained from the coordinate distances and combined to solve for the expansion rate $H(z)/H_0$ and acceleration rate $q(z)$ of the universe. The functions $H(y')$ and $q(y', y'')$ are exact, that is, they are not obtained by expansions in terms of derivatives about some point. The only assumption is that the universe is described by a Friedmann-Robertson-Walker (FRW) metric. The results are independent of the contents of the universe and their physical properties, and even independent of whether general relativity provides an accurate description of the universe. Here, we drop the assumption of zero space curvature, and it turns out that the deceleration parameter at a redshift of zero, q_0, remains the same, independent of whether space curvature is zero or not.

In this paper, we expand on the previous analysis done by Daly & Djorgovski (2003, 2004). First, we use updated and expanded data sets, as described in § 2.1. Second, we introduce a more direct way to compare the model-independent results obtained from the data with predictions; this is done by directly comparing the first and second derivatives of the coordinate distance with respect to redshift to predicted values in various models, as described in § 2.2. Third, we analyze the data using both a sliding window fit and fits in independent redshift bins. To solve for the physical properties of the dark energy as functions of redshift, a theory of gravity must be specified. To determine the properties of the dark energy, general relativity is taken to be the correct theory of gravity, allowing us to solve for the pressure, energy density, and equation of state of the dark energy as a function of redshift in § 2.4. Fourth, in § 2.4, we introduce a way to solve for the potential and kinetic energy densities of the dark energy as functions of redshift. In addition, we define a new model-independent function, the dark energy indicator, which provides a measure of deviations of w from -1 and a new and independent measure of Ω_m. Fifth, in § 2.3, these derivatives are combined to solve for the expansion and acceleration rates of the universe as functions of redshift for both zero and nonzero space curvature; in our previous work we have not considered the effects of nonzero space curvature. The only assumption that must be made to obtain the functions

TABLE 1
Distances 192 Supernovae, 30 Radio Galaxies, and 38 Galaxy Clusters

Type	Source	z	y	σ_y
SN	sn1994S	0.016	0.0160	0.0016
SN	sn2001V	0.016	0.0145	0.0015
SN	sn1996bo	0.016	0.0135	0.0015
SN	sn2001cz	0.016	0.0155	0.0017
SN	sn2000dk	0.016	0.0161	0.0016
SN	sn1997Y	0.017	0.0174	0.0018
SN	sn1998ef	0.017	0.0146	0.0016
SN	sn1998V	0.017	0.0160	0.0016
SN	sn1999ek	0.018	0.0155	0.0016
SN	sn1992bo	0.018	0.0190	0.0018

Note.—Table 1 is published in its entirety in the electronic edition of the *Astrophysical Journal*. A portion is shown here for guidance regarding its form and content.

$H(z)/H_0$ and $q(z)$ from the data are that the FRW metric is valid in our universe. A discussion and conclusions follow in § 3.

Other groups have explored complementary model-independent approaches to the study of the acceleration history of the universe. This includes the work of Huterer & Starkman (2003), Wang & Tegmark (2004, 2005), Shafieloo et al. (2006), Alam et al. (2004), Nesseris & Perivolaropoulos (2004), Huterer & Cooray (2005), Shapiro & Turner (2006), Turner & Huterer (2007), and Alam et al. (2007), for example. Summaries of these approaches are given by Sahni & Starobinsky (2006), Perivolaropoulos (2006), and Ratra & Vogeley (2007).

2. DATA AND ANALYSIS

2.1. *Data Sets Used*

We consider three types of distances: those determined from luminosity distances to supernova standard candles (SN), those determined from the angular diameter distances to radio galaxies (RG), and those determined to clusters of galaxies (CL) with Sunyaev-Zeldovich (SZ) measurements of angular diameter distances.

The SN samples studied here include those of Davis et al. (2007), Riess et al. (2007), and Astier et al. (2006); these authors provide the pertinent details about their measurements. There is some overlap between these supernovae samples, and this comparison allows the effects of different samples and subsamples to be seen. In addition, a comparison between the values of $y(z)$, $y'(z)$, and $y''(z)$ for the different samples goes hand in hand with a comparison of the best-fit parameter values obtained in different models for these same samples, described by Daly et al. (2008). The 71 new supernovae presented by Astier et al. (2006) are included in both the Riess et al. (2007) and Davis et al. (2007) samples, and the high-redshift *Hubble Space Telescope* (*HST*) supernovae of Riess et al. (2007) are included in the Davis et al. (2007) sample, which otherwise includes only ESSENCE supernovae and low-redshift supernovae. These comparisons can be quite helpful, as illustrated by the work of Nesseris & Perivolaropoulos (2007).

The dimensionless coordinate distance y and its uncertainty σ_y to a supernova can be obtained from the published distance modulus μ and its uncertainty σ_μ using the best-fit value of $\kappa_{\rm SN}$ and the relations $\mu = \kappa_{\rm SN} + 5\log[y(1+z)]$ and $\sigma_y = y\sigma_\mu[\ln(10)/5]$. There are several ways to determine $\kappa_{\rm SN} = 25 - 5\log(H_0/c)$ for published data sets for which the effective value of H_0 has not been determined (e.g., Daly et al. 2008). The different methods provide values of $\kappa_{\rm SN}$ that are in good agreement and, for cases for which the effective value of H_0 has been independently determined, such as in the work of Astier et al. (2006), the effective value of H_0 is recovered to very high accuracy. Here, we use the best-fit value of $\kappa_{\rm SN}$ obtained by Daly et al. (2008) for each source sample. We use the new RG sample of Daly et al. (2008); 11 new radio galaxies were observed and analyzed, which increases the sample size to 30 radio galaxies with redshifts between zero and about 1.8.

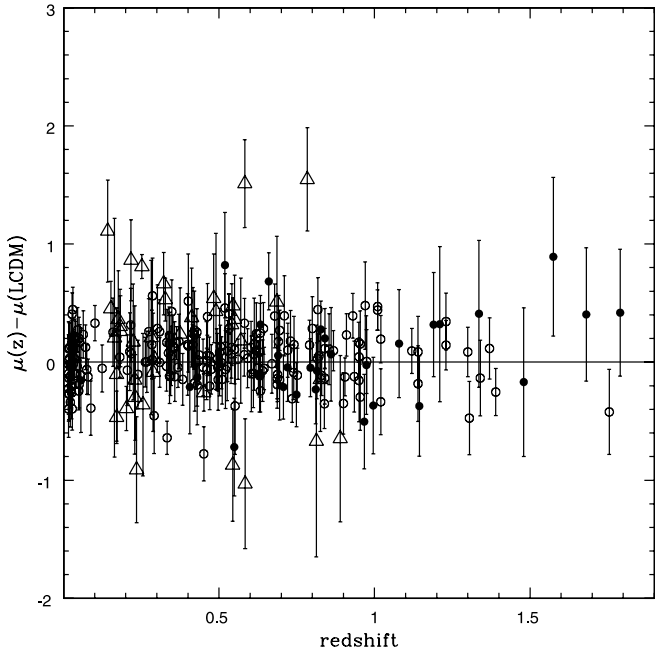

Fig. 1.—Difference between the distance modulus to the source and that expected in a standard LCDM model with $\Omega_m = 0.3$ and $\Omega_\Lambda = 0.7$. Open circles represent the 192 supernovae of Davis et al. (2007), filled circles represent the 30 radio galaxies of Daly et al. (2008), and open triangles represent the 38 clusters of Bonamente et al. (2006).

Finally, we also use the angular diameter distances to a sample of 38 clusters determined with the SZ measurements by Bonamente et al. (2006). The angular diameter distances d_A obtained by Bonamente et al. (2006) for the hydrostatic equilibrium model were used. To convert from the angular diameter distance to the dimensionless coordinate distance, we use the best-fit value of H_0 of $76.9^{+3.9}_{-3.4}$ km s^{-1} Mpc^{-1} obtained by Bonamente et al. (2006), to solve for the dimensionless coordinate distance y to each of their clusters using the well-known relations $d_A = (a_0 r)/(1+z)$ and $y = (H_0/c)(a_0 r)$.

After a detailed comparison between the SN and RG samples, we combine the Davis et al. (2007) supernova sample with the Daly et al. (2008) radio galaxy sample, and study the combined sample of 222 sources. Dimensionless coordinate distances y and their uncertainties $\sigma(y)$ are obtained for these samples as described by Daly et al. (2008), and are listed here in Table 1. We also study results obtained by adding the cluster sample of Bonamente et al. (2006) to obtain a sample of 260 sources; these distances are also included in Table 1. Figure 1 shows a comparison of the distances for these three data sets relative to the standard lambda cold dark matter (LCDM) model with $\Omega_m = 0.3$ and $\Omega_\Lambda = 0.7$. A comparison of each data set with the standard LCDM model indicates that both the SN and RG data sets provide reliable cosmology probes, while the SZ cluster method perhaps need some refinement; the reduced χ^2 for the SN and RG is ~1, as expected from the quoted measurement errors, whereas that for the SZ clusters is >2, suggesting that the quoted errors substantially underestimate the true uncertainties of these distance measurements.

However, to illustrate how our method can be applied to coordinate distances obtained using different methods, we consider the analysis of the full sample of 260 sources as well as the analysis of the sample of 222 SN and RG.

2.2. *Determinations of y' and y''*

The distances y to each source are used to obtain the distance $y(z)$ to any redshift within the redshift range of the sample, and first and second derivatives of the distance with respect to redshift, $y'(z)$ and $y''(z)$, and their uncertainties, using the method of Daly & Djorgovski (2003, 2004).

In previous work, we have used y' and y'' to obtain $E(z) = H(z)/H_0$ and $q(z)$. We then compared our empirically determined functions $E(z)$ and $q(z)$ with predictions in different models. However, it is also possible to compare our empirically determined functions $y'(z)$ and $y''(z)$ directly with model predictions for these quantities. The predicted values of these quantities are labeled y'_p and y''_p.

For a universe with nonrelativistic matter with normalized mean mass-energy density $\Omega_m(1+z)^3$, normalized mean dark energy density $\Omega_{\rm DE} f(z)$, and space curvature k in which Einstein's equations apply, we have, in full generality, the predicted values of y', y'_p, and y'', y''_p:

$$y'_p = \left[\frac{1+\Omega_k y_p^2}{\Omega_m(1+z)^3+\Omega_{\rm DE} f(z)+\Omega_k(1+z)^2}\right]^{1/2} \quad (1)$$

and

$$y''_p = \frac{y'_p}{(1+z)}\left[\frac{\Omega_k y_p y'_p(1+z)}{1+\Omega_k y_p^2} - 1.5\,\frac{\Omega_m(1+z)^3+\Omega_{\rm DE}(1+w)f(z)+(2/3)\Omega_k(1+z)^2}{\Omega_m(1+z)^3+\Omega_{\rm DE} f(z)+\Omega_k(1+z)^2}\right]. \quad (2)$$

Here $\Omega_k = -k/(H_0 a_0)^2$, $\Omega_m = \rho_{0m}/\rho_{0c}$ is the zero redshift value of the mean mass density of nonrelativistic matter relative to the critical density, $\Omega_{\rm DE} = \rho_{0\rm DE}/\rho_{0c}$ is the zero-redshift value of the dark energy density relative to the critical density, $\Omega_m + \Omega_{\rm DE} + \Omega_k = 1$, and $y_p = \int_0^z y'_p dz$ is obtained by numerically integrating equation (1). This derivation does not assume that $w = P_{\rm DE}/\rho_{\rm DE}$, is constant, and allows for variable $w(z)$. The function $f(z)$ describes the redshift evolution of the energy density of the dark energy; in a quintessence model with constant equation of state $w = P_{\rm DE}/\rho_{\rm DE}$, $f(z) = (1+z)^{3(1+w)}$, and for a cosmological constant $f(z) = 1$.

The data were analyzed using a sliding window fit, described in § 2.2.1, and using fits in independent redshift bins, described in § 2.2.2.

2.2.1. *Results Obtained with a Sliding Window Fit*

Fits are done using the window $\Delta z = 0.6$ throughout for the SN data, $\Delta z = 0.8$ for the RG data, when considered individually, and $\Delta z = 0.6$ for the joint samples using the method described by Daly & Djorgovski (2003, 2004). The width of the fitting window is driven by the need to obtain useful confidence intervals for the fits by including a sufficient number of data points. As the size of the available data sets increases in the future, this width could be correspondingly narrowed. In decreasing the window function width from 0.6 to 0.5 to 0.4, the trends and overall results remain the same, the uncertainties increase (because there are fewer data points in the window), and the trends become more noisy (due to sparser sampling). In addition, to test whether the window function has an effect on the trends extracted from the data, we created a mock data set with the same number and redshift distribution of points as in each data set and the same fractional error per point, but with y values obtained from a standard LCDM cosmology with $\Omega_m = 0.3$ and $\Omega_\Lambda = 0.7$ and ran it through the programs to extract $y(z)$, $y'(z)$, and $y''(z)$. As expected, the uncertainties increase as the window width decreases due to the smaller number of data points in the window. For window widths of 0.3 and 0.4 in redshift, $y(z)$, $y'(z)$, $y''(z)$, and $q(z)$ match the input cosmology to very high precision. For widths of 0.5 and 0.6, there is a very slight offset of $y''(z)$ and $q(z)$ from the input cosmology that sets in above redshifts of about 1, at a level that is very small compared with the uncertainties. Thus, the values of $y(z)$, $y'(z)$, $y''(z)$, and $q(z)$, and quantities obtained by combining these quantities, provide reliable determinations to redshifts well above 1.

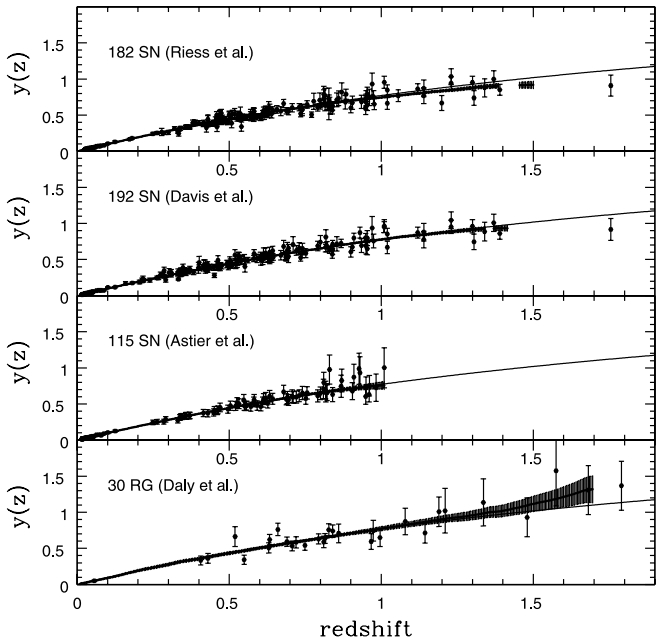

FIG. 2.—Dimensionless coordinate distances to each source, shown along with the best-fit $y(z)$ and its 1 σ error bar for the 182 gold supernovae from Riess et al. (2007), the 192 supernovae from Davis et al. (2007), the 115 supernovae of Astier et al. (2006), and the 30 radio galaxies from Daly et al. (2008). In this and in all subsequent figures, the solid curve illustrates the predicted value in a standard LCDM model with $\Omega_m = 0.3$ and $\Omega_\Lambda = 0.7$.

Our completely model-independent determinations of $y(z)$, $y'(z)$, and $y''(z)$ are shown in Figures 2–6. In Figures 2, 3, and 4, they are compared with the predicted value in a spatially flat universe, described by general relativity with a cosmological constant $\Omega_\Lambda = 0.7$, and nonrelativistic matter $\Omega_m = 0.3$. This provides a reasonable description of the data to redshifts of about 1 or so for the supernovae and 1.5 or so for the radio galaxies. (We note that this is not a model fit, but simply an illustration of its compatibility with the data.)

The values of $y'(z)$ and $y''(z)$ obtained for the Davis et al. (2007) supernova sample are compared with the best-fit model parameters obtained in a spatially flat quintessence model, a lambda model that allows for nonzero space curvature, and the standard LCDM model in Figures 5 and 6 using the best-fit model parameters listed by Daly et al. (2008). The best-fit model parameters are obtained by fitting the data to a model, and each model is based on general relativity. A comparison of the first and second derivatives of y

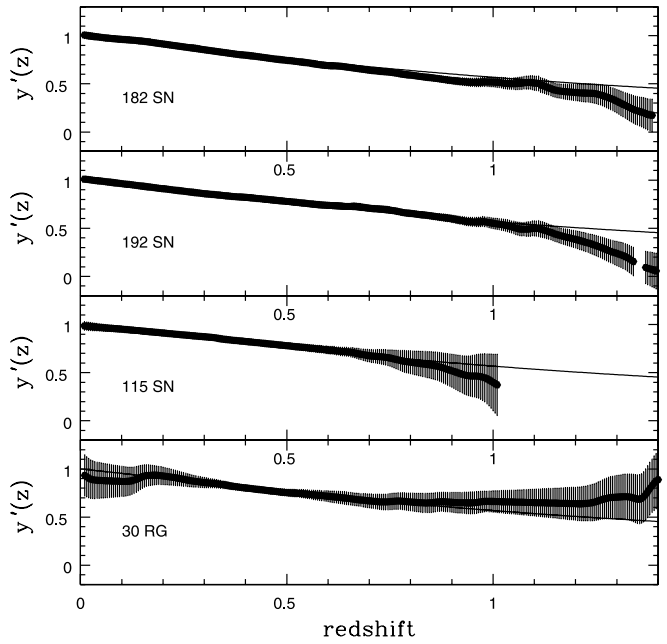

FIG. 3.—First derivative of the coordinate distance with respect to redshift as a function of redshift for the samples described in Fig. 2.

with those predicted in each of the models provides another way to see whether the model predictions provide a good description of the data. The models and best-fit model parameters are shown for a lambda model that allows for nonzero space curvature, and a quintessence model.

The comparison between the values of y' and y'' determined directly from the data with those predicted in a standard LCDM model that relies on the equations of general relativity provides effectively a large-scale test of general relativity. The good agreement obtained indicates that general relativity provides a good description of the data over look-back times (and the corresponding length scales) of about 10 billion years.

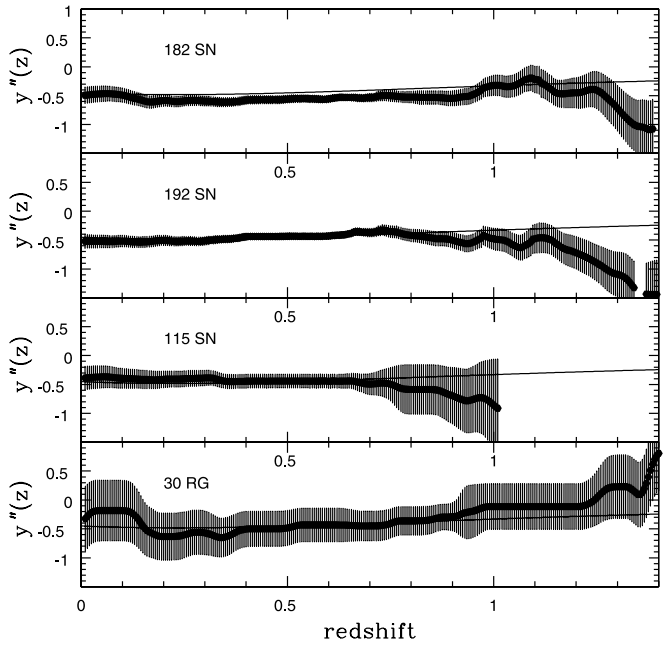

FIG. 4.—Second derivative of the coordinate distance with respect to redshift as a function of redshift for the samples described in Fig. 2.

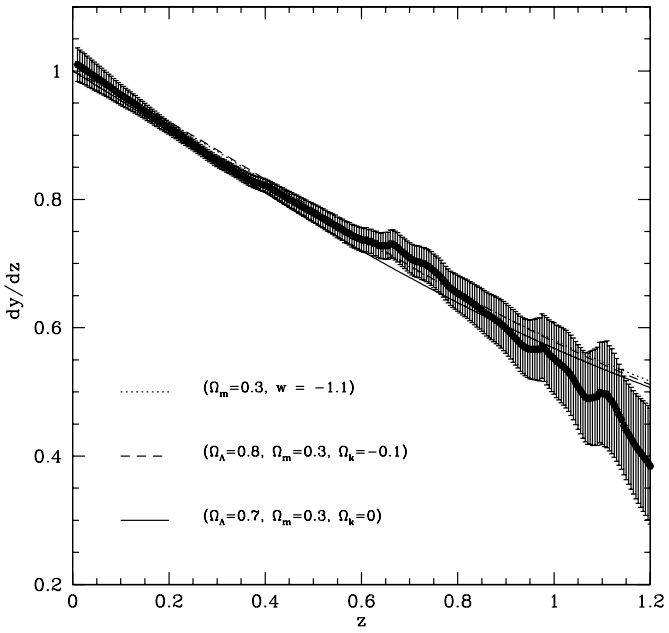

FIG. 5.—First derivative of the coordinate distance with respect to redshift as a function of redshift for the Davis et al. (2007) sample of 192 supernovae. Lines illustrating the predicted values of $y'(z)$, obtained by substituting the best-fit parameters of a spatially flat quintessence model, a lambda model with space curvature, and a standard flat LCDM model into eq. (1), are shown.

For the Davis et al. (2007) sample of 192 supernovae, the best-fit models track y' and y'' to a redshift of about 1.2 or so, beyond which the data drop away from the model prediction (see Figs. 5 and 6). Curves expected for the best-fit parameters obtained in a quintessence model and a cosmological constant model with space curvature by fitting $y(z)$, obtained by Daly et al. (2008), are shown as well as a standard LCDM model. For y' all three curves fit well, and some differences emerge for y''; in particular, the curve with nonzero space curvature does not fit the data well at low redshift.

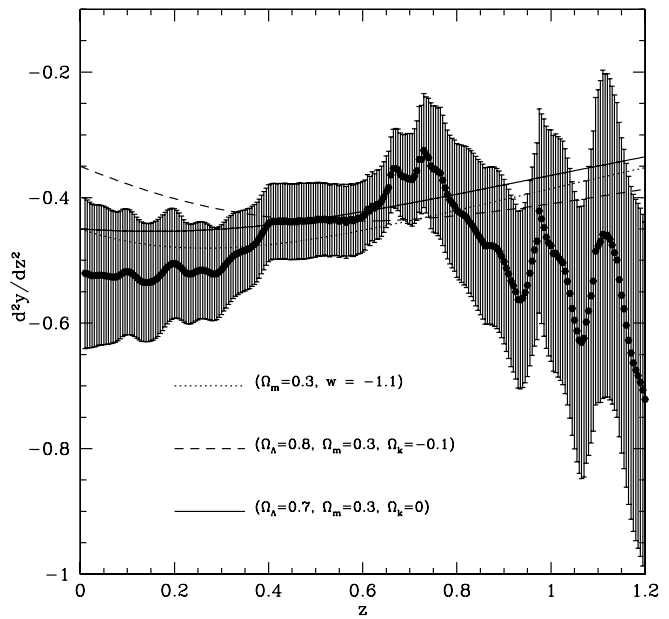

FIG. 6.—As in Fig. 5, but for the second derivative of the coordinate distance with respect to redshift. Lines illustrate the predicted values of $y''(z)$, obtained by substituting the best-fit parameters of a spatially flat quintessence model, a lambda model with space curvature, and a standard flat LCDM model into eq. (2).

TABLE 2
FITS IN INDEPENDENT REDSHIFT BINS TO 192 SUPERNOVAE AND 30 RADIO GALAXIES

Bin	N	$z_{\rm med}$	$z_{\rm min}$	$z_{\rm max}$	$y'(z_{\rm med})$	$H(z_{\rm med})/H_0$	$y''(z_{\rm med})$	$q(z_{\rm med})$
1/6	37	0.025	0.016	0.052	1.09 ± 0.05	0.92 ± 0.05	-6.2 ± 7.5	4.8 ± 6.9
2/6	37	0.275	0.054	0.348	0.74 ± 0.07	1.34 ± 0.13	-1.6 ± 0.8	1.9 ± 1.6
3/6	37	0.430	0.352	0.504	0.67 ± 0.15	1.48 ± 0.32	2.7 ± 6.5	...
4/6	37	0.600	0.508	0.670	0.72 ± 0.28	1.4 ± 0.5	1.2 ± 11	...
5/6	37	0.790	0.679	0.905	0.55 ± 0.16	1.8 ± 0.5	-4.0 ± 5.0	...
6/6	37	1.100	0.910	1.790	0.40 ± 0.13	2.5 ± 0.8	-0.4 ± 0.8	1.1 ± 3.7
1/4	55	0.035	0.016	0.268	1.03 ± 0.03	0.97 ± 0.03	-0.9 ± 0.6	-0.1 ± 0.6
2/4	55	0.400	0.274	0.502	0.79 ± 0.08	1.27 ± 0.13	-0.4 ± 2.5	-0.2 ± 4.5
3/4	55	0.630	0.504	0.749	0.54 ± 0.12	1.85 ± 0.40	-2.5 ± 3.2	...
4/4	57	0.965	0.752	1.790	0.64 ± 0.10	1.57 ± 0.23	-0.9 ± 0.5	1.80 ± 1.3
1/3	74	0.050	0.016	0.348	1.02 ± 0.03	0.98 ± 0.03	-1.05 ± 0.27	0.08 ± 0.26
2/3	74	0.505	0.352	0.670	0.80 ± 0.06	1.26 ± 0.09	0.9 ± 1.4	-2.7 ± 2.6
3/3	74	0.905	0.679	1.790	0.66 ± 0.06	1.52 ± 0.15	-0.8 ± 0.3	1.2 ± 0.9
1/2	111	0.275	0.016	0.504	0.84 ± 0.02	1.19 ± 0.03	-0.73 ± 0.16	0.10 ± 0.27
2/2	111	0.790	0.508	1.790	0.63 ± 0.04	1.59 ± 0.10	-0.40 ± 0.21	0.13 ± 0.57

2.2.2. *Results Obtained with Fits in Independent Redshift Bins*

Our sliding window fit method produces fit values that are strongly correlated over the redshift range corresponding to the fitting window, and are thus indicative of trends, but cannot be used simply to evaluate a statistical significance of any particular model. For that, we would need independent values at different redshifts. To this effect, we divided the data sample in a number of independent redshift bins (note that the data are *not* binned or averaged; the sample is divided into groups of points belonging to non-overlapping redshift bins). One drawback of this approach is that the numbers of data points in each bin is smaller, and thus the fit values are noisier. Another drawback is that the boundary values of the fits are not constrained, allowing for discontinuities in the values of $y(z)$, $y'(z)$, and $y''(z)$ at the bin boundaries, which physically makes no sense. This is the price of the statistical independence.

The dimensionless coordinate distances to the 192 supernovae of Davis et al. (2007) were combined with those to the 30 radio galaxies of Daly et al. (2008) to obtain a sample of 222 sources with redshift between 0.016 and 1.79. These data were divided into bins based on the redshifts of the points to be able to obtain independent determinations of y' and y'' and their uncertainties. The data were divided into redshift bins with roughly equal numbers of points per bin. We considered 2 bins with 111 points each; 3 bins with 74 points each; 4 bins with 55 points in the first three bins and 57 points in the highest redshift bin; and 6 bins with 37 points each. The bin, number of points per bin, median redshift of the points in the bin, and the minimum and maximum redshift of points within the bin are listed in Table 2. Points in each bin were used to determine the values of y' and y'' and their uncertainties at the median redshift of the bin.

The results for y' are shown in Figure 7 for 3, 4, and 6 bins; the redshift range of the points that went into the determination of y' at the median redshift $z_{\rm med}$ are indicated by the horizontal lines. Three theoretical curves are included on the figure. The dotted line is the curve predicted by the standard LCDM model with $\Omega_m = 0.3$, and the other two curves, which are nearly identical, are those predicted in the Cardassian model (Freese & Lewis 2002) and the generalized Chaplygin gas model (Kamenshchik et al. 2001; Bilic et al. 2002; Bento et al. 2002) shown for the best-fit parameters obtained by Bento et al. (2006) assuming a spatially flat universe.

The results obtained for y'' are shown in Figure 8 for 2 and 3 bins. The full set of results are listed in Table 2. Given the noise inherent in the data that are currently available, it is not possible to obtain meaningful results for y'' with a larger number of independent bins. With more data, we will be able to obtain this quantity in a larger number of independent redshift bins.

2.3. *Determinations of $H(z)/H_0$ and $q(z)$ for Zero Space Curvature*

The dimensionless expansion rate $E(z) \equiv H(z)/H_0$ and the deceleration parameter $q(z)$ can be constructed directly from the fist

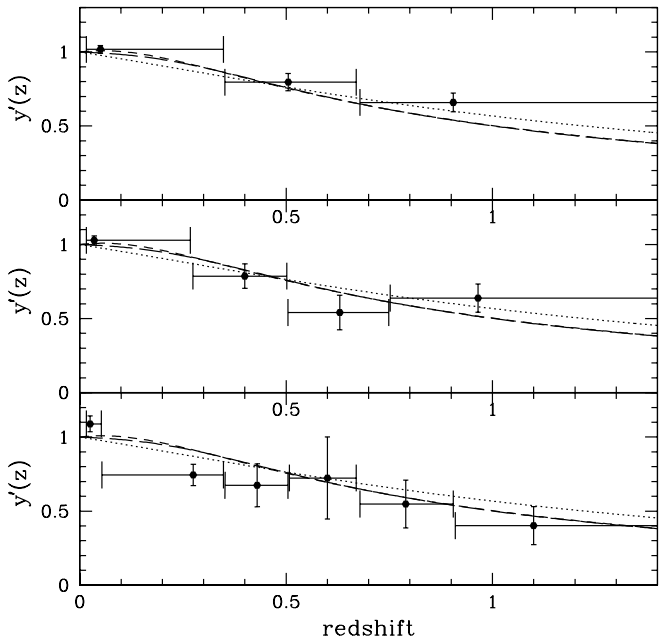

FIG. 7.—Results obtained for the first derivative of the coordinate distance with respect to redshift for the combined sample of 192 supernovae and 30 radio galaxies using data split into three bins (*top panel*), four bins (*middle panel*), and six bins (*bottom panel*). The data point at the median redshift is shown, and the horizontal bars indicate the redshift range of the data points in the bin. The standard LCDM prediction for $\Omega_m = 0.3$ is indicated by the dotted line, and the curves predicted by the Cardassian model and the generalized Chaplygin gas model, which yield nearly identical results, are shown by the short- and long-dashed curves, respectively.

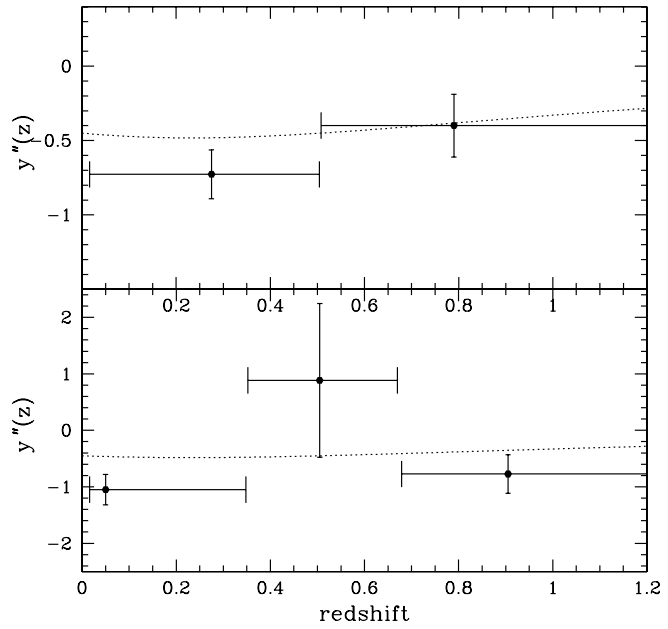

FIG. 8.—Results obtained for the second derivative of the coordinate distance with respect to redshift for the combined sample of 192 supernovae and 30 radio galaxies using data split into two bins (*top panel*) and three bins (*bottom panel*). The data point at the median redshift is shown, and the horizontal bars indicate the redshift range of the data points in the bin. The standard LCDM prediction for $\Omega_m = 0.3$ is indicated by the dotted line.

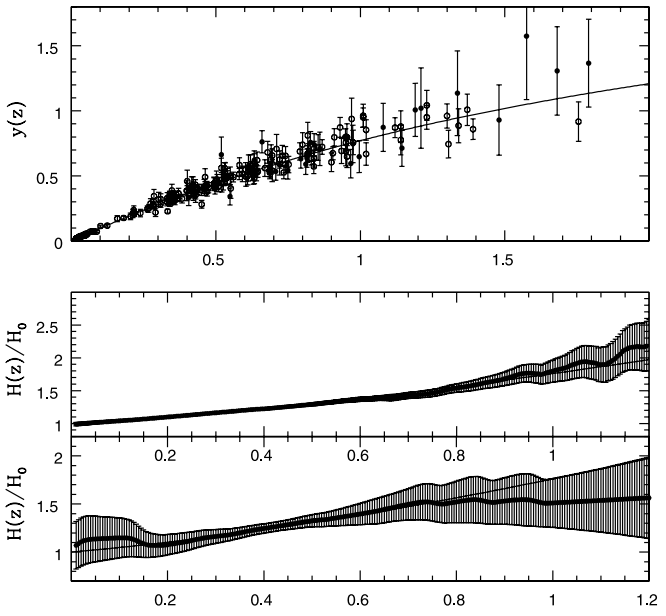

FIG. 9.—*Top*: Dimensionless coordinate distances to the 192 supernovae of Davis et al. (2007; *open circles*) and the 30 radio galaxies of Daly et al. (2008; *filled circles*). *Middle*: Our model-independent determination of $H(z)$, obtained using eq. (3) with zero space curvature, shown for the combined sample of 192 supernovae and 30 radio galaxies. *Bottom*: Same, but for 30 radio galaxies alone.

and second derivatives of the coordinate distance y' and y'', as discussed in detail by Daly & Djorgovski (2003). The relationship between $E(z)$ and y', and that between $q(z)$ and y' and y'', are exact; they do not represent expansions about some point. The only specification needed to derive these exact relationships is that the FRW line element is valid in our universe. With this assumption alone, it can be shown that

$$H(z)/H_0 = (y')^{-1}(1 + \Omega_k y^2)^{1/2} \tag{3}$$

(e.g., Weinberg 1972), and

$$q(z) = -1 - (1+z)y''(y')^{-1} + \frac{\Omega_k y y'(1+z)}{1+\Omega_k y^2} \tag{4}$$

(Daly & Djorgovski 2003), where $H(z) \equiv (\dot{a}/a)$, $q(z) \equiv -(\ddot{a}a)/(\dot{a})^2$, $\Omega_k \equiv -k/(H_0 a_0)^2$, and k is positive and Ω_k is negative when space curvature is positive. Thus, the zero redshift value of $q(z=0) = -1 - (y''/y')|_{z=0}$ is independent of space curvature, as is $E_0 = (1/y')|_{z=0}$, since $y = 0$ at $z = 0$. Thus, the zero redshift values of $E(z)$ and $q(z)$ obtained from y' and y'' are independent of space curvature. In addition, the zero redshift value of q indicates whether the universe is accelerating at the current epoch and can be determined independent of Ω_k.

2.3.1. *Results Obtained with a Sliding Window Fit*

The data and analysis described in § 2.2.1 were used to obtain $H(z)/H_0$ and $q(z)$ using equations (3) and (4) with $\Omega_k = 0$ (see § 2.5 for results with nonzero Ω_k). The results are shown in Figures 9 and 10 for the combined sample of 222 sources described above. The results confirm that the universe is accelerating at the current epoch. For the Davis et al. (2007) sample of 192 supernovae, we find a zero redshift value of q of $q_0(192\ \mathrm{SNe}) = -0.48 \pm 0.11$. For the radio galaxies, we find $q_0(30\ \mathrm{RG}) = -0.65 \pm 0.5$, consistent with the results obtained using supernovae. Again, these results depend only on the form of the FRW line element and are independent of space curvature, whether general relativity is the correct theory of gravity, and the content or evolution of the contents of the universe. For $k = 0$, the redshift at which the universe transitions from acceleration to deceleration for the Davis et al. (2007) sample of 192 SNe is $z_T = 0.77^{+0.11}_{-0.24}$.

We investigated the effect of the size of the window function of the value of q_0 and the transition redshift for the combined sample of 192 supernovae and 30 radio galaxies. For a window function of width 0.6 in redshift, we obtain $q_0 = -0.48 \pm 0.11$

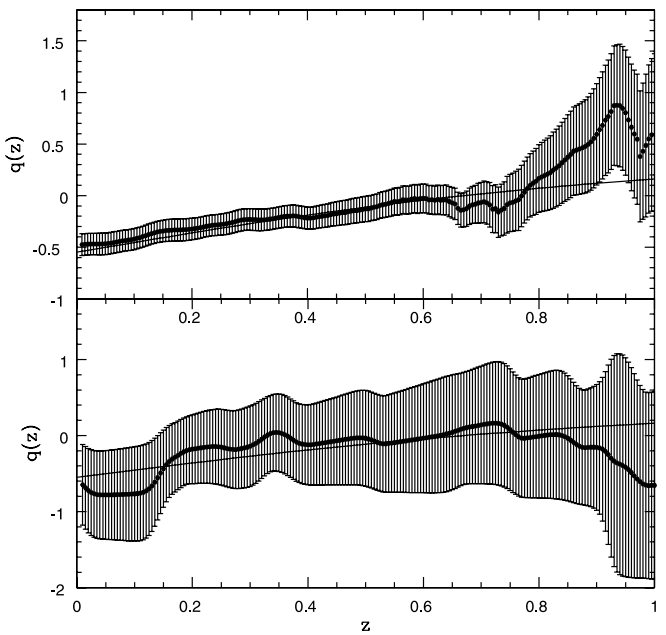

FIG. 10.—Our model-independent determination of $q(z)$, obtained using eq. (4) with zero space curvature, shown for the combined sample of 192 supernovae and 30 radio galaxies (*top*) and for 30 radio galaxies alone (*bottom*).

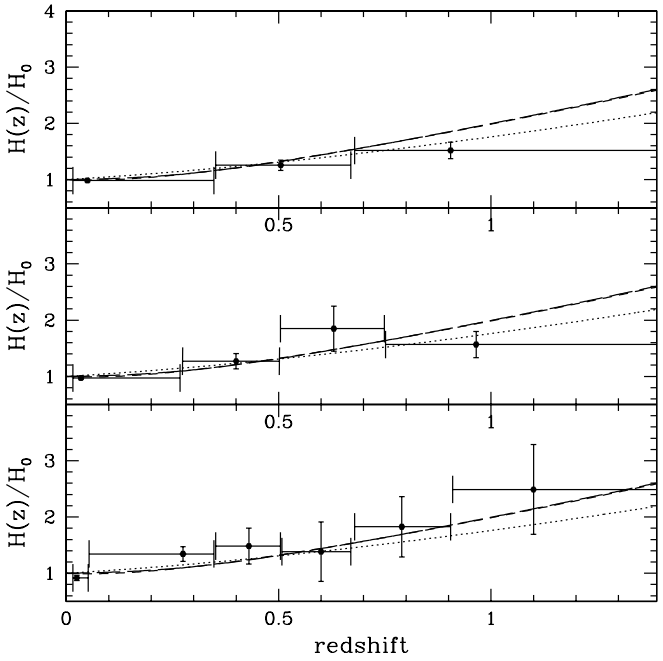

FIG. 11.—As in Fig. 7, but for $H(z_{\rm med})/H_0$, obtained using eq. (3) with zero space curvature.

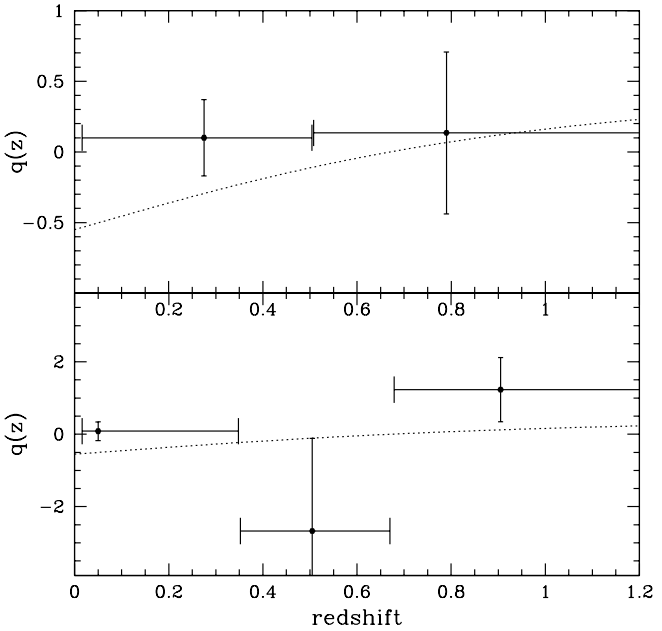

FIG. 12.—As in Fig. 8, but for $q(z_{\rm med})$, obtained using eq. (4) with zero space curvature.

and a transition redshift $z_T = 0.78^{+0.08}_{-0.27}$; for a window function of width 0.5 in redshift, we obtain $q_0 = -0.37 \pm 0.13$ and a transition redshift $z_T = 0.79 \pm 0.15$; and for a window function of width 0.4, we obtain $q_0 = -0.30 \pm 0.18$ and $z_T = 0.71 \pm 0.37$. These numbers are all consistent, although the uncertainties increase as the size of the window function decreases, since then fewer points are used to determine each quantity. It is important to increase the number of data points at all redshifts so that the size of the window function can be decreased. These transition redshifts are consistent with those obtained by other groups, such as Melchiorri et al. (2007) and Alam et al. (2007).

2.3.2. *Results Obtained with Fits in Independent Redshift Bins*

The data and analysis described in § 2.2.2 were used to obtain $H(z)/H_0$ and $q(z)$ using equations (3) and (4) with $\Omega_k = 0$ (see § 2.5 for results with nonzero Ω_k). The results are shown in Figures 11 and 12, and are listed in Table 2.

The values of $H(z_{\rm med})$ are consistent with predictions in the standard LCDM model at about 1 σ or better. For comparison, predictions obtained in a Cardassian model and generalized Chaplygin gas model, described in § 2.2.2, are also displayed. The value of the deceleration parameter at the median redshift of the bin, $q(z_{\rm med})$, does not definitely show that the universe is accelerating today, using this approach. That is, we do not see that q must be less than zero. If we consider the data split into two bins, each with 111 data points, and review the results for the lower redshift bin, we find that at a redshift of 0.02, the value of q is -0.28 ± 0.14. If we consider the data split into three bins, each with 74 data points, and review the results for the lowest redshift bin, we find that the value q is consistent with zero for all of the data points in this bin. Evidently, we do not yet have a sufficient density of data points even at a redshift less than about 0.5 to be able to definitely state at 3 σ or better that the universe is accelerating today, using this method (fits in independent redshift bins). It is only when we increase the number of data points that go into the determination of $q(z)$ by using the sliding window function that we can conclude that the universe is accelerating today using our model-independent analysis.

Of course, when it is concluded that the universe is accelerating today in the context of a quintessence model or other models, all of the data are being used in the context of that particular model. The quintessence and most other models implicitly assume that our universe is described by the FRW line element, that the equations of general relativity apply, and that a specific function for the redshift evolution of the dark energy is valid over the redshift interval under study. Many more data are needed in order to test independently these (perfectly reasonable) assumptions.

2.4. *Determinations of the Properties of the Dark Energy*

We can solve for the properties of the dark energy as functions of redshift if a theory of gravity is specified, as shown by Daly & Djorgovski (2004). Einstein's equations of general relativity are used to relate the pressure, $P_{\rm DE}$, energy density, $\rho_{\rm DE}$, equation of state $w = P_{\rm DE}/\rho_{\rm DE}$, and potential, $V_{\rm DE}$, and kinetic, $K_{\rm DE}$, energy densities as functions of redshift to the cosmic scale factor a, and the first and second derivatives of a with respect to time. Since the FRW line element has been used to relate the first and second derivatives of a with respect to time to the first and second derivatives of the coordinate distance with respect to redshift, y' and y'', the equations of general relativity can be used to solve for the pressure, energy density, equation of state, and potential and kinetic energy density of the dark energy in terms of y' and y'', which are obtained directly from the data. Here a value of $k = 0$ is assumed, and the equations of Daly & Djorgovski (2004) are used to solve for the properties of the dark energy as functions of redshift. To obtain the pressure, we only need to specify that Einstein's equations apply,

$$\frac{P_{\rm DE}(z)}{\rho_{0c}} = -(y')^{-2}\left[1 + \tfrac{2}{3}(1+z)y''(y')^{-1}\right]. \qquad (5)$$

As pointed out by Daly & Djorgovski (2004), the zero redshift value of P translates into a value of Ω_Λ in a standard LCDM model, since in this model $w = -1$, so $\Omega_\Lambda = \rho_{\rm DE}/\rho_{0c} = -P_0/\rho_{0c}$. Here, this implies that $\Omega_\Lambda = 0.64 \pm 0.1$ if the dark energy is due

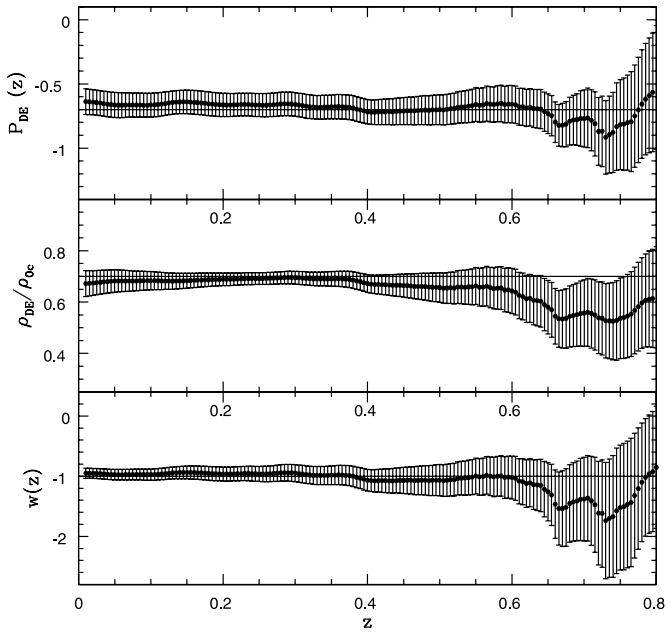

FIG. 13.—Pressure, energy density, and equation of state of the dark energy for the combined sample of 30 radio galaxies and 192 supernovae, obtained from y' and y'' using eqs. (5), (6), and (7), respectively, assuming $\Omega_m = 0.3$ in eqs. (6) and (7).

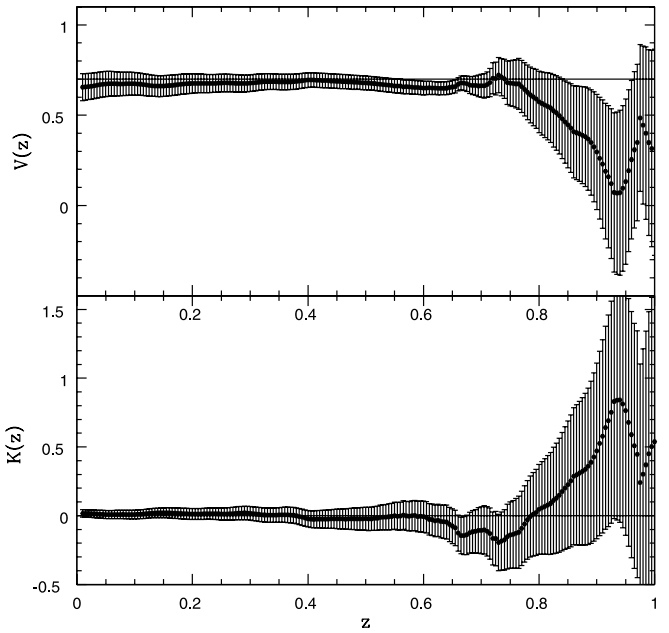

FIG. 14.—Potential and kinetic energy density of a dark energy scalar field for the combined sample of 30 radio galaxies and 192 supernovae, obtained from y' and y'' using eqs. (8) and (9), respectively, assuming $\Omega_m = 0.3$.

to a cosmological constant in a universe with zero space curvature. This value of Ω_Λ, which is obtained from the first and second derivatives of the coordinate distance, is consistent with other measures.

To obtain the energy density $\rho_{\rm DE}$ of the dark energy, Ω_m must be specified, and a value of $\Omega_m = 0.3$ is adopted here:

$$\frac{\rho_{\rm DE}(z)}{\rho_{0c}} = (y')^{-2} - \Omega_m(1+z)^3. \tag{6}$$

The equation of state w is obtained by taking the ratio $P_{\rm DE}/\rho_{\rm DE}$ and is given by

$$w(z) = \frac{-[1+(2/3)(1+z)y''(y')^{-1}]}{1-\Omega_m(1+z)^3(y')^2}. \tag{7}$$

The potential energy density of a dark energy scalar field is given by $V = 0.5(\rho - P)$, so

$$\frac{V_{\rm DE}(z)}{\rho_{0c}} = (y')^{-2}\left[1+\frac{(1+z)y''}{3y'}\right] - 0.5\Omega_m(1+z)^3 \tag{8}$$

and the kinetic energy density is given by $K = 0.5(\rho + P)$, so

$$\frac{K_{\rm DE}}{\rho_{0c}} = \frac{-y''(1+z)}{3(y')^3} - 0.5\Omega_m(1+z)^3, \tag{9}$$

since $V = 0.5(\rho - P)$ and $K = 0.5(\rho + P)$.

We define a new model-independent function, the dark energy indicator s, which is given by

$$s = \frac{y''}{(y')^3(1+z)^2}. \tag{10}$$

The function is model-independent, because no assumptions have been adopted to arrive at this function; it is valid independent of a theory of gravity and the contents (and space curvature) of the universe. This choice for s is motivated by the fact that, for zero space curvature, the predicted value of s is

$$\begin{aligned} s_p &= -1.5\Omega_m\left[1+(1+w)\frac{\Omega_{\rm DE}f(z)}{\Omega_m(1+z)^3}\right] \\ &= -1.5\Omega_m\left[1+(1+w)\frac{\rho_{\rm DE}}{\rho_m}\right], \end{aligned} \tag{11}$$

as indicated by equations (1) and (2); this occurs because $y_p'' \propto (y_p')^3(1+z)^2$ when $\Omega_k = 0$. Equation (11) is derived assuming that general relativity is valid, space curvature is zero, and there are two mass-energy components controlling the expansion of the universe: dark energy and nonrelativistic matter including dark matter and baryons. It is not assumed that the equation of state of the dark energy, w, is constant, and no functional form for the evolution of the energy density of the dark energy, $f(z)$, is assumed. If $w = -1$, then $s_p = -1.5\Omega_m$, and the value of s obtained using equation (10) provides a new and independent measure of Ω_m. Deviations of s from a constant provide a measure of the deviations of w from -1; the amount of the deviation also depends on the ratio of the energy density of the dark energy $\rho_{\rm DE}(z)$ to that of the mass density of nonrelativistic matter $\rho_m(z)$, including dark matter and baryons, at a given redshift, as discussed in more detail below.

2.4.1. *Results Obtained with a Sliding Window Fit*

The analysis described in § 2.2.1 was applied to the combined sample of 192 supernovae from Davis et al. (2007) and 30 radio galaxies from Daly et al. (2008). The values of y' and y'' were substituted into equations (5), (6), (7), (8), (9), and (10), and the results are shown in Figures 13, 14, and 15. The zero redshift values of these parameters are $P_0/\rho_{0c} = -0.64 \pm 0.10$, $\rho_{\rm DE}(z=0)/\rho_{0c} = 0.67 \pm 0.05$, $w_0 = -0.95 \pm 0.08$, $V_0/\rho_{0c} = 0.65 \pm 0.05$, $K_0/\rho_{0c} = 0.01 \pm 0.03$, and $s_0 = -0.50 \pm 0.08$. The zero redshift value of s indicates a value of $\Omega_m = 0.33 \pm 0.05$ if $w = -1$, and the zero redshift value of P indicates a value of

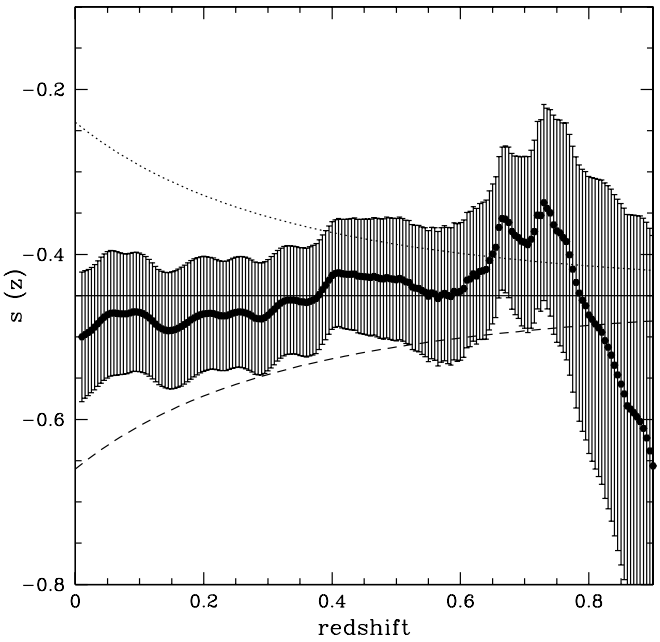

FIG. 15.—Dark energy indicator for the combined sample of 30 radio galaxies and 192 supernovae obtained using eq. (10). The behavior of s predicted by eq. (11) is shown for three simple models each with $\Omega_m = 0.3$, $\Omega_{\rm DE} = 0.7$, and $f(z) = 1$ over the redshift range shown, and $w = -1$ (*solid line*), $w = -0.8$ and remains constant (*long-dashed curve*), and $w = -1.2$ and remains constant (*short-dashed curve*). If s is constant, it suggests that $w = -1$, and the value of s provides a new and independent measure of Ω_m.

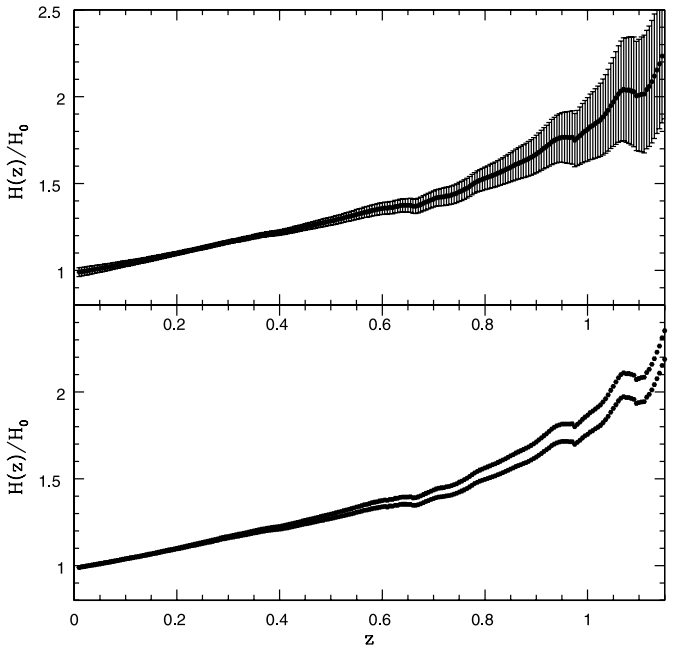

FIG. 16.—Model-independent determination of $H(z)$ for the Davis et al. (2007) sample of 192 supernovae obtained using eq. (3). The top panel shows results obtained for $\Omega_k = 0$, and the bottom panel shows results obtained for $\Omega_k = 0.1$ (*upper curve*) and $\Omega_k = -0.1$ (*lower curve*). For clarity, the uncertainties are not shown in the bottom panel, but are similar to those shown in the top panel.

$\Omega_\Lambda = 0.64 \pm 0.10$ if $w = -1$. Overall, the results are consistent with predictions in a standard LCDM model.

As noted above, the dark energy indicator s provides a measure of whether $w = -1$ over the redshift range shown in Figure 15. To illustrate the signature of a value of w that differs from -1, three curves are overlaid on the figure. Each curve is obtained using equation (11) assuming $\Omega_m = 0.3$, $\Omega_{\rm DE} = 0.7$, $f(z) = 1$, and $w =$ const. over the redshift range shown, with values of w of -1.2 (*short-dashed curve*), $w = -1$ (*solid line*), and $w = -0.8$ (*long-dashed curve*). Clearly, the curves with $w = -0.8$ and $w = -1.2$ do not provide a good description of the data. Another way to look at this is that equations (10) and (11) indicate that $w = -1 - (\rho_m/\rho_{\rm DE})[2s/(3\Omega_m) + 1]$, so the second part of this is a measure of the deviation of w from -1. At zero redshift the ratio $\rho_m/\rho_{\rm DE} \sim 0.3/0.7$ and $\Omega_m = 0.3$, so s places rather strong constraints on deviations of w_0 from -1. For example, with $s_0 = -0.50 \pm 0.08$ obtained above, $w_0 = -0.95 \pm 0.08$, for $\Omega_m = 0.3$. A zero redshift value of w of -1 would suggest that $w = -1$ for all redshifts, or that w asymptotes to -1 at late times.

Since most of these functions involve combinations of the first and second derivatives of the coordinate distance, results obtained with independent redshift bins are quite noisy, so only values obtained in two independent redshift bins are listed in Table 3.

2.5. *Effect of Space Curvature on $H(z)/H_0$ and $q(z)$*

The dimensionless expansion rate $H(z)/H_0$ and the deceleration parameter $q(z)$ can be obtained assuming only the validity of the FRW metric using equations (3) and (4), allowing for reasonable values of space curvature. Space curvature, parameterized by Ω_k, has only a modest effect on $H(z)$ and $q(z)$ for reasonable values of Ω_k, as illustrated in Figures 16 and 17 for the Davis et al. (2007) sample of 192 SNe. Positive values of Ω_k cause $H(z)$ to increase more steeply with redshift than negative values of Ω_k, which tend to flatten out the $H(z)$ curve. Positive space curvature, with negative Ω_k, flattens the $q(z)$ curve and pushes the redshift at which the universe transitions from an accelerating state to a decelerating state to higher redshift. This follows, since y' is known to be positive in our universe, since the universe is expanding. Similarly, negative space curvature moves the redshift at which $q = 0$ to lower redshift, causing the universe to transition from an accelerating to a decelerating state at lower redshift. For $k = 0$, the redshift at which the universe transitions from acceleration to deceleration for the Davis et al. (2007) sample is $z_T = 0.77^{+0.11}_{-0.24}$. For negative space curvature with $\Omega_k = 0.1$, this transition redshift is shifted to about 0.6, and for positive space curvature with $\Omega_k = -0.1$ it shifts to about 0.8. Thus, the effect of space curvature on $H(z)$ and $q(z)$ is small relative to the overall uncertainties of their measurements, for a plausible range of the curvature parameter Ω_k.

2.6. *Determinations of y' and y'' for Other Samples*

We also consider the full sample of 260 sources, including the 38 SZ clusters of Bonamente et al. (2006), the 192 supernovae of Davis et al. (2007), and the 30 radio galaxies of Daly et al. (2008). These results are shown in Figure 18; a window function

TABLE 3
FITS IN INDEPENDENT REDSHIFT BINS AT THE MEDIAN REDSHIFT OF THE BIN

Data	$P_{\rm DE}/\rho_{0c}$	$\rho_{\rm DE}/\rho_{0c}$	$w_{\rm DE}$	$V_{\rm DE}/\rho_{0c}$	$K_{\rm DE}/\rho_{0c}$	s
1/2	-0.38 ± 0.24	0.79 ± 0.07	-0.48 ± 0.34	0.58 ± 0.10	0.21 ± 0.15	-0.75 ± 0.21
2/2	-0.6 ± 1.0	0.8 ± 0.3	-0.8 ± 1.2	0.7 ± 0.6	0.1 ± 0.45	-0.50 ± 0.25

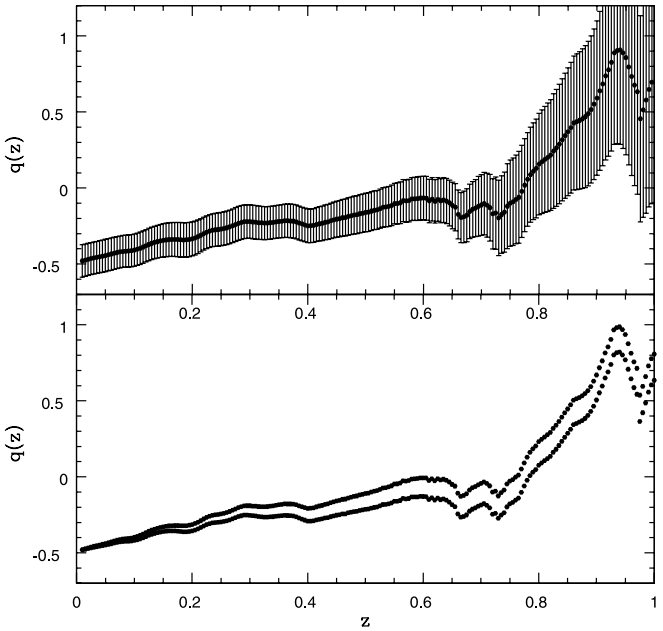

FIG. 17.—Model-independent determination of $q(z)$ for the Davis et al. (2007) sample of 192 supernovae obtained using eq. (4). The top panel shows results obtained for $\Omega_k = 0$, and the bottom panel shows results obtained for $\Omega_k = 0.1$ (*upper curve*) and $\Omega_k = -0.1$ (*lower curve*). For clarity, the uncertainties are not shown in the bottom panel, but are similar to those shown in the top panel.

of width 0.6 was used to analyze the data. This analysis illustrates how this method can be applied to diverse data sets. However, while the SZ cluster distances currently provide a useful tool for measurements of the far-field Hubble parameter, it is probably premature to use them as standard rulers to probe the global geometry and kinematics of the universe at this time.

Gamma-ray bursts as standard candles have been analyzed in detail by Schaefer (2007), who gives other pertinent references.

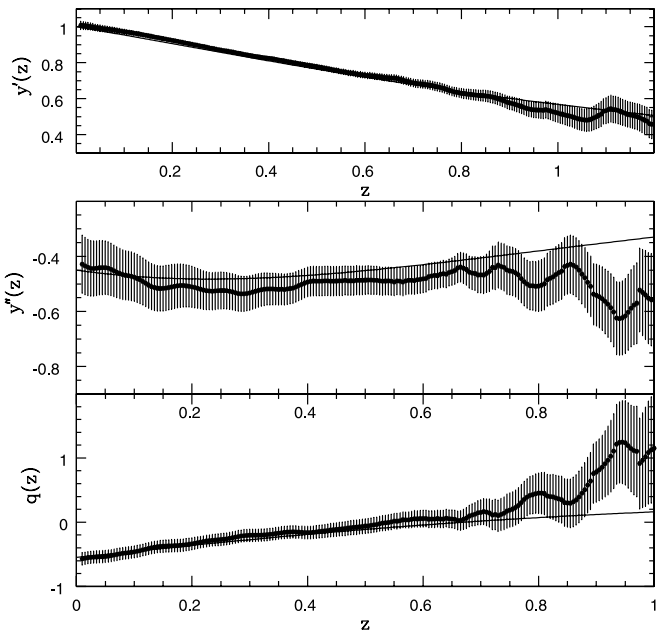

FIG. 18.—Results for $y'(z)$, $y''(z)$, and $q(z)$ (obtained using eq. [4] with zero space curvature) for the combined sample of 30 radio galaxies (*filled circles*), 192 supernovae (*open circles*), and 38 SZ clusters (*stars*), shown in Fig. 1. The solid curve illustrates the predicted value in a standard LCDM model with $\Omega_m = 0.3$ and $\Omega_\Lambda = 0.7$.

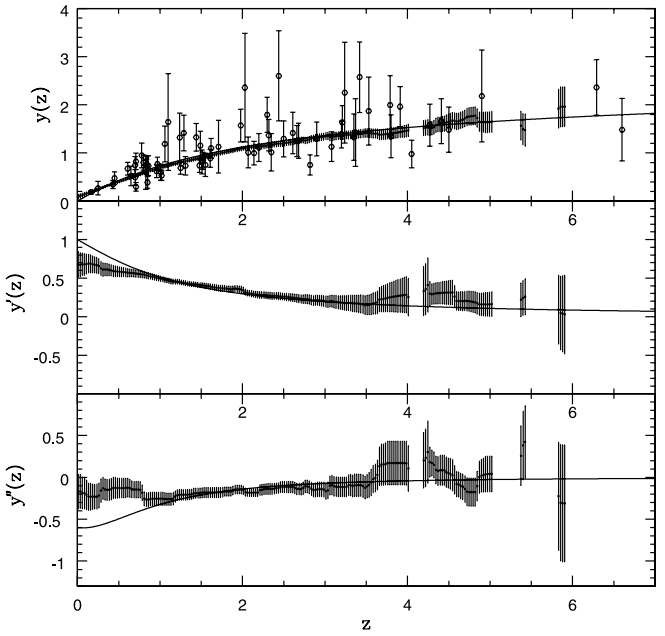

FIG. 19.—Results for $y(z)$, $y'(z)$, and $y''(z)$ obtained with the 69 gamma-ray burst data of Schaefer (2007). The solid curve illustrates the predicted value in a standard LCDM model with $\Omega_m = 0.4$ and $\Omega_\Lambda = 0.6$, which are the best-fit values to this model obtained by Schaefer (2007).

The values of μ listed by Schaefer (2007) can be used to determine the dimensionless coordinate distance to each source if the value of H_0 relevant for the sample is known, as described in § 2.1; here a value of $H_0 = 70$ km s^{-1} Mpc^{-1} was used (B. E. Schaefer 2007, private communication). The dimensionless coordinate distances were analyzed to determine the functions $y(z)$, $y'(z)$, and $y''(z)$ using a window function of width 2.0 in redshift. A first look at results for the gamma-ray bursts are shown in Figure 19, which suggests that these are a potentially promising tool to study cosmology at very large distances, and are broadly consistent with predictions in the canonical LCDM model. However, the quality and sparsity of the data indicate that it is still not sufficient for model-independent analysis, as shown above for the SN+RG sample, and there are reservations concerning the method as discussed, for example, by Friedman & Bloom (2005).

3. SUMMARY AND CONCLUSIONS

The work presented here improves and extends our previous results. First, expanded and improved data sets are considered, including three supernova samples and one radio galaxy sample. The radio galaxy data set has 11 new sources, increasing its size to 30 sources, and the supernovae data sets have increased substantially in size and quality. In addition, SZ cluster distances and gamma-ray burst distances are considered. The dimensionless coordinate distances (obtained directly from the data) and first and second derivatives of the distance are obtained as functions of redshift using a sliding window fit. The good agreement obtained using supernovae and radio galaxies, two completely independent methods, with sources that cover similar redshift ranges, suggests that neither method is strongly affected by systematic effects, and that each method provides a reliable cosmological tool.

The first and second derivatives of the distance are combined to obtain the acceleration parameter $q(z)$, allowing for nonzero space curvature. It is shown that the zero redshift value of $q(z)$, q_0, is independent of space curvature, and can be obtained from the first and second derivatives of the coordinate distance. Thus, q_0, which indicates whether the universe is accelerating at the

current epoch, can be obtained directly from the supernova and radio galaxy data; our determinations of $q(z)$ only relies on the validity of the FRW line element, and is independent of a theory of gravity and the contents of the universe. Each of the supernova samples and the radio galaxy sample, analyzed using a sliding window fit, indicates that the universe is accelerating today independent of space curvature, independent of whether general relativity is the correct theory of gravity, and independent of the contents of the universe. The effect of nonzero space curvature on $q(z)$ is to shift the redshift at which the universe transitions from acceleration to deceleration, moving this to lower redshift for negative space curvature and to higher redshift for positive space curvature. The zero redshift values of q obtained using a sliding window fit for the Davis et al. (2007) supernova sample is $q_0(192\ \mathrm{SNe}) = -0.48 \pm 0.11$, and that obtained for the radio galaxy sample of Daly et al. (2008) is $q_0(30\ \mathrm{RG}) = -0.65 \pm 0.53$, indicating that the universe is accelerating at the current epoch. The data were also binned so that only certain subsets of the data were used to solve for y', y'', $H(z)/H_0$, and $q(z)$. The results for y' and $H(z)/H_0$ indicate that the standard LCDM model provides a good description of the data. The results for y'' and $q(z)$ are consistent with the standard LCDM model, but do not independently confirm the model or the acceleration of the universe.

In addition to the evaluation of the standard cosmological parameters, in an even more direct approach, we compared y' and y'' obtained from the fits to the data to model predictions. Comparisons of y' and y'' with predictions based on general relativity indicate that general relativity provides an accurate description of the data on look-back timescales of about 10 billion years, thus providing a very large scale test of general relativity.

Another new approach is that the data were analyzed using both a sliding window fit and fits in independent redshift bins. The fits in statistically independent redshift bins are broadly consistent with the sliding window fits, but are generally noisier (as expected).

We also explored the effects of nonzero space curvature on determinations of $H(z)$ and $q(z)$. It is shown that the zero redshift value of q, obtained by applying equation (4) to y' and y'', is independent of space curvature. This means that our method can be used to determine q_0, and thus the degree to which the universe is accelerating at the current epoch, with only one assumption, that the FRW line element is valid. In addition, it is found that the effect of space curvature on the shape of $H(z)$ and $q(z)$ is small, relative to the uncertainties arising from the measurement errors.

After determining the expansion and acceleration rates of the universe as functions of redshift independent of a theory of gravity, we solve for the pressure, energy density, equation of state, and potential and kinetic energy of the dark energy as functions of redshift, assuming that general relativity is the correct theory of gravity. We also define a new model-independent function, the dark energy indicator s, which provides a measure of deviations of the equation of state of the dark energy w from -1, and provides a new and independent measure of Ω_m if $w = -1$. The results obtained using a sliding window fit indicate that a cosmological constant in a spatially flat universe provides a good description of each of these quantities over the redshift range from 0 to 1. The zero redshift values of these quantities obtained with the Davis et al. (2007) supernova sample are $P_{\mathrm{DE},0}/\rho_{0c} = -0.64 \pm 0.10$, $\rho_{\mathrm{DE},0}/\rho_{0c} = 0.67 \pm 0.05$, $w_{\mathrm{DE},0} = -0.95 \pm 0.08$, $V_{\mathrm{DE},0}/\rho_{0c} = 0.65 \pm 0.05$, $K_{\mathrm{DE},0}/\rho_{0c} = 0.01 \pm 0.03$, and $s_0 = -0.50 \pm 0.08$. In the standard LCDM model, $\Omega_\Lambda = -P_0/\rho_{0c} = 0.64 \pm 0.1$, obtained using the first and second derivatives of the coordinate distance, provides an independent measure of Ω_Λ. In addition, in this model, $w = -1$, so s provides a measure of Ω_m, and the value obtained here using the first and second derivatives of the coordinate distance is $\Omega_m = 0.33 \pm 0.05$. Overall, the shapes of the pressure, energy density, equation of state, and other parameters as functions of redshift are consistent with those predicted in a standard LCDM model. There is a tantalizing hint that there may be deviations from the standard model at high redshift; more observations at high redshift will be needed to investigate this further. The results obtained using fits in independent redshift bins are consistent with the standard LCDM model, but do not independently confirm the model.

We would like to thank the observers for their tireless efforts in obtaining the data used for this study. We would also like to thank the referee for very helpful comments and suggestions. This work was supported in part by US National Science Foundation grants AST-0507465 (R. A. D.) and AST-0407448 (S. G. D.), and the Ajax Foundation (S. G. D.).

REFERENCES

Alam, U., Sahni, V., & Starobinsky, A. A. 2004, J. Cosmol. Astropart. Phys., 06, 008
———. 2007, J. Cosmol. Astropart. Phys., 0702, 11
Astier, P., et al. 2006, A&A, 447, 31
Bento, M. C., Bertolami, O., Santos, N. M. C., & Sen, A. A. 2006, J. Phys. Conf. Ser., 33, 197
Bento, M. C., Bertolami, O., & Sen, A. A. 2002, Phys. Rev. D, 66, 043507
Bilic, N., Tupper, G. B, & Viollier, R. D. 2002, Phys. Lett. B, 535, 17
Bonamente, M., Joy, M. K., LaRoque, S. J., Carlstrom, J. E., Reese, E. D., & Dawson, K. S. 2006, ApJ, 647, 25
Daly, R. A. 1994, ApJ, 426, 38
Daly, R. A., & Djorgovski, S. G. 2003, ApJ, 597, 9
———. 2004, ApJ, 612, 652
Daly, R. A., Mory, M. P., O'Dea, C. P., Kharb, P., Baum, S., Guerra, E. J., & Djorgovski, S. G. 2008, ApJ, in press (arXiv:0710.5112)
Davis, T. M., et al. 2007, ApJ, 666, 716
Freese, K., & Lewis, M. 2002, Phys. Lett. B, 540, 1
Friedman, A. S., & Bloom, J. S. 2005, ApJ, 627, 1
Hamuy, M., Phillips, M. M., Maza, J., Suntzeff, N. B., Schommer, R. A., & Aviles, R. 1995, AJ, 109, 1
Huterer, D., & Cooray, A. 2005, Phys. Rev. D., 71, 023506
Huterer, D., & Starkman, G. 2003, Phys. Rev. Lett., 90, 031301
Kamenshchik, A. Y., Moschella, U., & Pasquier, V. 2001, Phys. Lett. B, 511, 265
Melchiorri, A., Pagano, L., & Pandolfi, S. 2007, Phys. Rev. D, 76, 041301
Nesseris, S., & Perivolaropoulos, L. 2004, Phys. Rev. D, 70, 043531
———. 2007, J. Cosmol. Astropart. Phys., 0702, 25
Perivolaropoulos, L. 2006, in AIP Conf. Ser. 848, Recent Advances in Astronomy and Astrophysics (New York: AIP), 698
Phillips, M. M. 1993, ApJ, 413, L105
Ratra, B., & Vogeley, M. S. 2007, preprint (arXiv:0706.1565)
———. 2007, ApJ, 659, 98
Sahni, V., & Starobinsky, A. 2006, Int. J. Mod. Phys. D, 15, 2105
Schaefer, B. E. 2007, ApJ, 660, 16
Shafieloo, A., Alam, U., Sahni, V., & Starobinsky, A. 2006, MNRAS, 366, 1081
Shapiro, C., & Turner, M. S. 2006, ApJ, 649, 563
Turner, M. S., & Huterer, D. 2007, J. Phys. Soc. Japan, 11, 111015
Wang, Y., & Tegmark, M. 2004, Phys. Rev. Lett., 92, 241302
———. 2005, Phys. Rev. D, 71, 103513
Weinberg, S. 1972, Gravitation and Cosmology (New York: Wiley)
Wood-Vasey, W. M., et al. 2007, ApJ, 666, 694